Dendritic Spike Induction of Postsynaptic Cerebellar LTP

Marco Canepari and Kaspar E. Vogt

Division of Pharmacology and Neurobiology, Biozentrum – University of Basel,

Klingelbergstrasse 70, CH-4056 Basel, Switzerland

Correspondence to:

Dr. Marco Canepari

Division of Pharmacology and Neurobiology, Biozentrum – University of Basel,

Klingelbergstrasse 70, 4056 Basel, Switzerland

Tel.: +41 (61) 2672179 Fax: +41 (61) 2672179

E-mail: marco.canepari@unibas.ch

Running Title:

Calcium Spikes induce Cerebellar LTP

Additional information on the manuscript:
Number of words in the main text: 3,959
Number of Words in the Summary: 150
Number of figures: 8

Note: Supplementary Information is included

ABSTRACT

The architecture of parallel fiber (PF) axons contacting cerebellar Purkinje neurons (PNs) retains spatial information over long distances. PF synapses can trigger local dendritic calcium spikes, but whether and how this calcium signal leads to plastic changes that decode the PF input organization is unknown. By combining voltage and calcium imaging, we show that PF-elicited calcium signals, mediated by voltage-gated calcium channels, increase non-linearly during high-frequency bursts of electrically constant calcium spikes because they locally and transiently saturate the endogenous buffer. We demonstrate that these non-linear calcium signals, independently of NMDA or metabotropic glutamate receptor activation, can induce PF long-term potentiation (LTP). Two-photon imaging in coronal slices revealed that calcium signals inducing LTP can be observed by stimulating either the PF or the ascending fiber pathway. We propose that local dendritic calcium spikes, evoked by synaptic potentials, provide a unique mechanism to spatially decode PF signals into cerebellar circuitry changes.

Neuronal dendrites fire action potentials mediated by voltage-gated calcium channels (VGCC) that can be sufficient to induce long-term potentiation of synaptic potentials [1,2]. Calcium signals mediated by VGCCs differ from those mediated by ionotropic or metabotropic glutamate receptors. Whereas the latter signals co-localize with activated receptors, either by direct calcium influx or by secondary intracellular pathways, the extent of the former signals is determined by the spread of the dendritic spike. In the cerebellar Purkinje neuron (PN), calcium spikes can be elicited by parallel fiber (PF) stimulation and can be localized to small regions [3]. However, the function of calcium spikes elicited by neighboring presynaptic fibers is unknown. In particular, dendritic excitation has been associated with PF synaptic plasticity in relation to the climbing fibre (CF)-EPSP providing the calcium signal underlying coincident PF and CF detection and PF-LTD [4], but the role of local PF-elicited calcium spikes in long-term synaptic plasticity is unexplored.

In this report we show that PF-elicited dendritic calcium spikes can induce postsynaptic PF-LTP in the mouse cerebellum. We demonstrate that this phenomenon is correlated with the ability of high-frequency calcium spike bursts to locally and transiently saturate the endogenous calcium buffer (ECB) leading to supra-linear summation of intracellular free calcium concentration changes ($\Delta[Ca^{2+}]_i$). Since dendritic excitation depends on the spatiotemporal summation of synaptic inputs, the present results suggest that a major physiological role of PF-evoked dendritic calcium spikes is to functionally associate cerebellar granule cell axons synchronously targeting the same PN dendritic region.

RESULTS

Dendritic calcium spikes and non-linear summation of calcium signals elicited by PF-EPSPs

Dendritic membrane potential and calcium signals were optically investigated in mouse cerebellar sagittal slices. We measured dendritic changes in membrane potential (ΔV_m) and in intracellular free calcium concentration ($\Delta[Ca^{2+}]_i$) signals in PNs loaded with the voltage sensitive dye JPW-1114 and 1 mM of the low-affinity calcium indicator Fura-FF as previously described [5]. High frequency trains of PF-EPSPs can elicit calcium spikes that mediate $\Delta[Ca^{2+}]_i$ which depend on the number of stimuli [6]. In the example of **Fig. 1a**, PF stimulation in the vicinity of a dendritic branch with 3, 5, 7 and 10 pulses at 100 Hz elicited local ΔV_m and $\Delta[Ca^{2+}]_i$ signals which declined sharply with the distance from the site of stimulation. In the burst of 10 EPSPs, the somatic response facilitated from ~5 mV to ~20 mV after the third pulse with episodes of somatic action potentials. The somatic EPSPs were comparable to those measured in the majority of the dendritic field. However, in the area where $\Delta[Ca^{2+}]_i$ signals were detected, the peak ΔV_m signal exceeded 40 mV (**Fig. 1b**), indicating dendritic calcium spikes [7,3]. Notably, the size of the dendritic calcium spike associated with the 3rd-10th EPSP did not change, but the $\Delta[Ca^{2+}]_i$ increased supra-linearly with the number

of events. This result was observed in all 5 PNs tested for 3-10 PF EPSPs (**Fig. 1c**).

The supra-linear $\Delta[Ca^{2+}]_i$ signal described above was due to two factors as shown in the experiment in **Fig. 1d** where $\Delta[Ca^{2+}]_i$ signals were analyzed for 3 and 7 EPSPs. First, the contribution to the $\Delta[Ca^{2+}]_i$ signal of each calcium spike increased during the burst. Second, the fast component of the decay time constant (τ) of the $\Delta[Ca^{2+}]_i$ signals decreased with the number of EPSPs, enhancing the summation of $\Delta[Ca^{2+}]_i$ contributions from individual spikes. In **Fig. 1e** the $\Delta[Ca^{2+}]_i$ signals associated with the 3rd and 7th EPSPs are superimposed and normalized to their maxima. Single exponential functions are fitted to the initial 20 ms decay of the two $\Delta[Ca^{2+}]_i$ signals. In contrast to the marked change in the $\Delta[Ca^{2+}]_i$ signal, the difference in the peak ΔV_m signal associated with the 3rd and 7th EPSPs was minimal. As shown in **Fig. 1f**, in 8 cells with peak $\Delta[Ca^{2+}]_i$ signal of 0.7-1.5 µM after 7 PF-EPSPs, the $\Delta[Ca^{2+}]_i$ contribution of the 7th EPSP spike, relative to the 3rd, was higher (ratio: 1.66±0.22; paired t-test $p<0.01$) and the decay time constant of the $\Delta[Ca^{2+}]_i$ signal after 7 EPSPs, relative to the $\Delta[Ca^{2+}]_i$ signal after 3 EPSPs, slower (ratio: 1.98±0.51; paired t-test $p<0.01$). However, the peak ΔV_m associated with the 7th EPSP, relative to the peak ΔV_m associated with the 3rd EPSP, was not different (ratio: 1.00±0.03, paired t-test $p>0.2$), indicating no change in the calcium spikes during the burst.

The peak $\Delta[Ca^{2+}]_i$ signal followed the calcium spike by 2-4 ms, suggesting calcium spike influx independent of mGluR1-mediated signals or of influx via NMDA receptors, expressed in mature PNs [8]. Pharmacological tests reported in

the **Supplementary Results** demonstrate that fast $\Delta[Ca^{2+}]_i$ signals associated with PF-stimulation spikes are mediated by VGCCs.

The size of the $\Delta[Ca^{2+}]_i$ transients increases with the number of stimulated PF terminals and therefore with the excited dendritic area [6]. **Fig. 2a** shows one example of a PN where ΔV_m and $\Delta[Ca^{2+}]_i$ signals were measured following PF stimulation at two different intensities. The area of dendritic excitation and of the observable $\Delta[Ca^{2+}]_i$ signal enlarged with the stronger stimulation. In the region excited by the weaker stimulation, the peak $\Delta[Ca^{2+}]_i$ increased with the stronger stimulation (**Fig. 2b**), but the peaks of ΔV_m corresponding to the last spikes did not change (**Fig. 2c**). The same result was observed in 7 cells tested with two stimulation intensities, as shown in the scatter plot of **Fig. 2d**.

This first set of experiments shows that the non-linear $\Delta[Ca^{2+}]_i$ increase associated with PF-evoked dendritic spikes is independent of the electrical amplitude of the calcium spike.

Dendritic calcium spikes and calcium signals elicited by CF-EPSPs

Dendritic calcium spikes can be also elicited by CF-EPSPs [9], but they are spread over a large area of the dendritic tree. In another set of experiments we examined whether and how supra-linear calcium signals can occur following CF stimulation.

CF-EPSP bursts are dominated by short-term depression due to presynaptic depletion [10,11]. In the experiment shown in **Fig. 3a**, ΔV_m and $\Delta[Ca^{2+}]_i$ signals following either 1 CF-EPSP or 5 CF-EPSPs were measured. The peak ΔV_m

signals corresponding to the 2^{nd}-5^{th} EPSP were smaller compared to the first one. In most dendritic regions, the first EPSP of the train evoked a calcium spike, but nowhere was the dendrite excited by the 2^{nd}-5^{th} EPSP. In 4 cells, we measured ΔV_m and $\Delta[Ca^{2+}]_i$ signals over the whole imaged dendritic area. The peak ΔV_m signals of the 1^{st}, 2^{nd}, 3^{rd}, 4^{th}, and 5^{th} EPSP were 43.0±4.2 mV, 29.0±2.4 mV, 30.0±5.0 mV, 29.3.0±5.0 mV and 28.5±3.7 mV respectively, whereas the $\Delta[Ca^{2+}]_i$ signal following 1 CF-EPSPs and 5-CF EPSPs were unaltered (168±50 nM and 165±50 nM respectively, **Fig. 3b**). Therefore, CF-EPSP bursts are associated with small dendritic $\Delta[Ca^{2+}]_i$ signals because only the first EPSP of a train can evoke a calcium spike.

Although CF-mediated $\Delta[Ca^{2+}]_i$ signals are small, when paired with a short delay after PF-EPSPs bursts, CF-EPSPs are associated with a supra-linear dendritic $\Delta[Ca^{2+}]_i$ signal, independent of the activation of mGluR1s and calcium release from stores [12]. Therefore, we tested whether the ΔV_m signal associated with the CF-EPSP was changed by the pairing protocol. **Fig. 3c** shows one experiment in which ΔV_m and $\Delta[Ca^{2+}]_i$ signals were measured for a pairing protocol with one CF-EPSP delayed by 90 ms from the beginning of a 7 PF-EPSPs burst. In the region of PF-evoked dendritic calcium spikes, the $\Delta[Ca^{2+}]_i$ signal associated with the CF-EPSP increased during the pairing protocol (**Fig. 3d**). The site of the supra-linear $\Delta[Ca^{2+}]_i$ signal (**Fig. 3e**), obtained as the difference between the $\Delta[Ca^{2+}]_i$ signals during paired and unpaired stimulation, co-localized with the region of the PF-evoked dendritic spikes (**Fig. 3c**). However, the dendritic depolarization associated with the CF-EPSP did not

change following the pairing protocol (**Fig. 3e**), indicating that the previous PF-EPSPs burst did not affect the CF-evoked calcium spike. In 6 cells (**Fig. 3f**), in the region excited by the PF-EPSPs burst, the paired peak CF-associated $\Delta[Ca^{2+}]_i$, obtained by subtracting the PF- $\Delta[Ca^{2+}]_i$ from the paired $\Delta[Ca^{2+}]_i$, was 433±33 nM, higher ($p<0.01$, two-sample t-test) than the unpaired peak CF $\Delta[Ca^{2+}]_i$ (192±50 nM). In contrast, the paired peak CF ΔV_m (43.5±7.7 mV) did not change from the unpaired CF ΔV_m (45.7±8.3 mV, $p>0.2$ two-sample t-test). Therefore, the dendritic supra-linear calcium signal, associated with paired PF and CF stimulation, is independent of the ΔV_m peak of the CF-evoked calcium spike.

PF-evoked dendritic spikes induce PF long-term synaptic plasticity

High-frequency PF-evoked calcium spikes produce progressively larger $\Delta[Ca^{2+}]_i$ components after the 2^{nd}-4^{th} spike. This phenomenon is independent of the electrical amplitude of dendritic calcium spikes excluding the possibility of increasing calcium influx later in the spike train. The only remaining possibility for a $\Delta[Ca^{2+}]_i$ increase is the progressive saturation of calcium binding proteins forming the ECB, because our experiments also ruled out calcium release from stores. To confirm this conclusion, we directly estimated the amount of calcium influx in experiments reported in the **Supplementary Results**.

To test whether the transient ECB saturation is correlated with induction of synaptic plasticity, we explored the effect of repetitive bursting activity on the amplitude of the PF-EPSPs, recorded every 15 s (4 EPSPs every minute, 0.067

Hz). In the experiment of **Fig. 4a**, we first tested the changes in the PF-EPSP amplitude induced by repeating (60 times at 1 Hz) first 3 PF-EPSPs bursts (typically $\Delta[Ca^{2+}]_i$ below ECB saturation) and later 7 PF-EPSPs bursts ($\Delta[Ca^{2+}]_i$ above ECB saturation). In a 8X8 pixels region, 3 EPSPs were associated with 2 calcium spikes and a $\Delta[Ca^{2+}]_i$ signal of ~200 nM whereas 7 EPSPs were associated with 6 calcium spikes and a $\Delta[Ca^{2+}]_i$ signal of ~900 nM (**Fig. 4b**). Repetitive application of 3 EPSPs didn't cause any change in the EPSP amplitude tested up to 15 minutes later, whereas repetitive application of 7 EPSPs caused a robust LTP (**Fig. 4c-d**). The scatter plot and the bar diagram of **Fig. 4e** show the fractional change of the EPSP amplitude 10-15 minutes following repetitive stimulation with 3 and 7 EPSPs (summary results from 6 cells). 3 EPSPs which evoked peak $\Delta[Ca^{2+}]_i$ signals <300 nM never affected the EPSP amplitude whereas 7 EPSPs associated with peak $\Delta[Ca^{2+}]_i$ signals >600 nM consistently caused LTP.

To characterize the long-term synaptic plasticity induced by PF-evoked dendritic spikes we used a standard protocol (conditioning protocol) of 7 EPSPs at 100 Hz (EPSP burst) repeated 60 times at 1 Hz. By adjusting the stimulation intensity, we explored the effect of $\Delta[Ca^{2+}]_i$ signals of different size. To standardize the analysis, we correlated the 8X8 pixel region of maximal $\Delta[Ca^{2+}]_i$ size, ranging from 0.1 µM (the minimal detectable $\Delta[Ca^{2+}]_i$) up to 4 µM, with the amplitude of the PF-EPSPs.

Fig. 5 shows three representative experiments with conditioning protocols adjusted to obtain peak $\Delta[Ca^{2+}]_i$ signals of ~0.2 µM, ~1 µM and ~2 µM. In the first

example (**Fig. 5a-b**), the amplitude of the PF-EPSPs, after a transient post-tetanic potentiation, returned to the initial EPSP amplitude after ~2 minutes. In the second example (**Fig. 5c-d**), the transient post-tetanic potentiation was followed by an LTP of the PF-EPSPs lasting for more than 20 minutes. In the last example (**Fig. 5e-f**) the conditioning protocol induced a long-term depression (LTD) of the PF-EPSP, lasting for more than 20 minutes. The scatter plot of **Fig. 5g** summarizes the changes in PF-EPSP amplitudes as a function of the peak $\Delta[Ca^{2+}]_i$ after 5-10 minutes obtained from 34 cells for a total of N=45 dendritic locations tested. The graph of **Fig. 5h** reveals a novel quantitative dependence of plasticity from the dendritic $\Delta[Ca^{2+}]_i$ signal. In the range of 0.1-0.4 μM the PF-EPSP was occasionally potentiated but in the majority of the cases it was not affected by the conditioning protocol (changes in EPSP amplitude after 5-10 minutes and after 15-20 minutes: 1.14±0.20, N=14 and 1.15±0.25, N=6, respectively). In contrast, in the range of 0.4 – 1.5 μM, the PF-EPSP was consistently potentiated by the conditioning protocol (change in EPSP amplitude after 5-10 minutes and after 15-20 minutes 1.39±0.20, N=20) and 1.42±0.17, N=10, respectively). Finally, in the larger range of 2 – 4 μM the conditioning protocol consistently induced LTD (change in the EPSP amplitude after 5-10 minutes and after 15-20 minutes: 0.67±0.13, N=8 and 0.58±0.07, N=4, respectively).

The profile of long-term plasticity as a function of the $\Delta[Ca^{2+}]_i$ signal during the conditioning protocol was maintained in the presence of the mGluR1 antagonists CPCCOEt (100 μM, 7 cells and N = 12 dendritic locations) or LY367385 (100 μM,

8 cells and N=12 dendritic locations) and of the NMDA receptor antagonist AP5 (100 µM, 10 cells and N=13 dendritic locations). In the presence of CPCCOEt, LY367385 and NMDA respectively, the fractional change in EPSP amplitude in the range of 0.4 – 1.5 µM was 1.47±0.24 (N=8), 1.49±0.30 (N=7) and 1.51±0.22 (N=9) after 5-10 minutes and 1.45±0.15 (N=4), 1.40±0.17 (N=4) and 1.53±0.19 (N=4) after 20 minutes, whereas in the range of 2 – 4 µM the fractional change after 5-10 minutes was 0.64±0.28 (N=4), 0.65±0.15 (N=4) and 0.60±0.18 (N=4). Stimulation in control conditions could involve long-term plasticity mediated by inhibitory synaptic potentials. To test this hypothesis in 7 cells (N=10 dendritic locations) we did experiments in the presence of the $GABA_A$ receptor antagonist bicuculline (20 µM). The fractional change in EPSP amplitude in the range of 0.4 – 1.5 µM was 1.50±0.29 (N=6) after 5-10 minutes and 1.51±0.36 (N=4) after 20 minutes, whereas in the range of 2 - 4 µM it was 0.79±0.28 (N=4) after 5-10 minutes, indicating no effect of bicuculline.

The definitive confirmation that LTP is exclusively mediated by calcium influx via VGCCs requires the application of the conditioning protocol during a complete block of postsynaptic calcium transients. To this aim, we loaded PNs with 25 mM BAPTA and 100 µM Alexa-488 after filling the tip of the patch pipette with BAPTA-free solution to allow measurements of $\Delta[Ca^{2+}]_i$ signals before BAPTA diffusion. In the experiment of **Fig. 6a**, we positioned two stimulation electrodes as the dendrite became visible with the Fura-FF fluorescence (~2 minutes after breaking the seal) and measured $\Delta[Ca^{2+}]_i$ associated with EPSP bursts every ~30 s. The amplitude of the $\Delta[Ca^{2+}]_i$ signal, adjusted to be in the

LTP range, was constant for ~10-15 minutes. After the first detection of Alexa fluorescence in the dendrite (**Fig. 6a**), we waited ~35 minutes to allow for dendritic BAPTA equilibration and to test the conditioning protocol. No LTP was observed. The same result was obtained with two stimulating electrodes in 6 experiments (**Fig. 6b**). **Fig. 6c** shows the scatter plot of the EPSP change 5-10 minutes after the conditioning protocol relative to the initial value against the $\Delta[Ca^{2+}]_i$ signal in the presence of BAPTA, together with the data points in control conditions in the range of 0.4 – 1 µM $\Delta[Ca^{2+}]_i$. With intracellular BAPTA, the fractional change of the EPSP amplitude was 1.00±0.09 (N=6), smaller than that observed in control conditions (1.38±0.19, N=13, $p<0.01$ two-sample t-test).

Altogether, these experiments demonstrate that PF-LTP is induced postsynaptically by the conditioning protocol. Other experiments reported in the **Supplementary Results** indicate that this PF-LTP also has a postsynaptic expression.

PF-evoked and AF-evoked dendritic firing and LTP in coronal slices

It has been shown that PF synapses and synapses from cerebellar granule cells (CGCs) formed in the ascending tract [13] have different susceptibility for synaptic plasticity [14,15]. This phenomenon was attributed to the different spatial arrangements of PF and AF afferents [16]. To discriminate PF and AF inputs, we did experiments in coronal slices as described by Sims and Hartell [14,15] and by Marcaggi and Attwell [16]. In this preparation, the organization of synaptic inputs is preserved and the dendritic plane of PNs is perpendicular to the slice with a

variable descending angle (Fig. 7*A*). We selected those neurons with dendrites positioned at an angle of ~30º-45º from the slice plane and imaged the entire dendrite over multiple planes to localize and quantify $\Delta[Ca^{2+}]_i$ signals using two-photon microscopy. We used the non-ratiometric low-affinity indicator Oregon Green BAPTA-5N (OG-5N) and calibrated its fluorescence change against Fura-FF (**Fig. 7b**) in order to compare calcium fluorescence signals.

In the first series of experiments (N=7 cells), we positioned the stimulating electrode in the molecular layer (ML) ~150 µm from the monitored PN to stimulate PFs. In the experiment of **Fig. 7c**, after having localized the scanning plane with the largest dendritic $\Delta[Ca^{2+}]_i$ signal, we recorded calcium fluorescence over small areas evoked by EPSP bursts at different stimulation intensities. PF-EPSP bursts locally excited the dendrite leading to $\Delta[Ca^{2+}]_i$ signals in the micromolar range (**Fig. 7d**). The relation between the amplitude of the first EPSP and the $\Delta[Ca^{2+}]_i$ signal was almost linear up to EPSPs of ~9 mV and $\Delta[Ca^{2+}]_i$ signals of ~2 µM in all the 7 cells tested (**Fig. 7e**). In general, we observed that $\Delta[Ca^{2+}]_i$ signals that are expected to induce LTP were always associated with EPSP bursts in which the amplitude of the first EPSP was in the range of 3-6 mV.

In the second series of experiments (N=6 cells), we positioned the stimulating electrode in the granule cell layer (GCL) behind the monitored PN allowing for AF stimulation. In the experiment of **Fig. 7f**, the AF-EPSP bursts, although sparser, could still evoke dendritic spikes (**Fig. 7g**). In all the cells, compared to the PF stimulation, $\Delta[Ca^{2+}]_i$ signals were smaller, not linearly related with the first EPSP

amplitude (**Fig. 7h**) and generally less localized. These signals, however, could still reach values compatible with LTP induction.

In the final set of experiments – which did not include calcium measurements - we tested the conditioning protocol, applied either to the PF or to the AF pathways in coronal slices. We adjusted the stimulation intensity to obtain the first EPSP amplitude of 3-6 mV, leading to $\Delta[Ca^{2+}]_i$ signals in the expected PF-LTP range. For PF stimulation (N=6 cells), the conditioning protocol induced LTP (fractional change of EPSP amplitude after 15-20 minutes: 1.56±0.21), whereas no change in the PF-EPSP amplitude was observed in another set of 6 neurons filled with 25 mM BAPTA (fractional change of EPSP amplitude after 15-20 minutes: 0.99±0.07) as shown in **Fig. 8a-b**. We repeated the same test for AF-EPSPs (N=6 cells in control internal and N=6 cells with 25 mM BAPTA) using the same EPSP amplitude. LTP was also observed for AF-EPSPs (fractional change of EPSP amplitude after 10-15 minutes: 1.45±0.19), but not in the cells filled with BAPTA (fractional change of EPSP amplitude after 10-15 minutes: 1.01±0.04) as shown in **Fig. 8c-d**.

In summary, dendritic calcium spikes and associated LTP were detected following both PF and AF stimulation.

DISCUSSION

In this report, we describe three novel findings that significantly further our understanding of the dendritic mechanisms underlying PN synaptic plasticity. First, we show that local high-frequency dendritic spikes generate $\Delta[Ca^{2+}]_i$ signals that summate non-linearly because they transiently saturate the ECB. Second, we demonstrate that this signal induces postsynaptic PF-LTP. Third, we report that dendritic calcium firing leading to LTP can occur not only by activation of adjacent PF-EPSPs, but also by activity in the sparser AF tract, implying a less stringent spatial organization of synaptic inputs compared to the one necessary for mGluR1- and endocannabinoid-mediated PF-LTD [17].

Dendritic calcium spikes can saturate the endogenous calcium buffer.

The ability of a cell to dynamically regulate calcium depends on the kinetic properties of the calcium-binding proteins forming the ECB as well as on the time course of the calcium signal [18]. When more spikes occur sequentially, $\Delta[Ca^{2+}]_i$ signals summate non-linearly if the associated calcium influx partially saturates calcium-binding molecules. Transient ECB saturation has been shown to occur presynaptically and to contribute to short-term plasticity [19]. Here, we show that it can occur postsynaptically leading to long-term synaptic plasticity. The evidence that the amplitude of the $\Delta[Ca^{2+}]_i$ signal depends on the size of the activated dendritic region suggests that the saturated ECB involves mostly mobile molecules re-equilibrating over relatively small volumes. The PN is characterized by an exceptionally large equilibrium buffering capacity estimated at ~2000 [20]. Both slow calcium-binding proteins like parvalbumin [21], and fast-binding

calcium-binding protein like Calbindin-D28k [22] contribute to the equilibrium ECB of PNs [23]. The present data doesn't provide an indication on which molecules are involved. However, in a different system, it has been shown that a calcium transient with increased amplitude and slower decay can be attributed to saturation of the slow-binding mobile buffer parvalbumin [24]. Our experimental approach allowed to observe that the supra-linear summation of $\Delta[Ca^{2+}]_i$ signals is independent of the increase in calcium influx per spike providing a demonstration for ECB saturation.

Dendritic calcium spikes can induce long-term plasticity

In this report, we observed that several consecutive dendritic spikes at 100 Hz can induce PF-LTP. Postsynaptic PF-LTP is necessary as a reversal mechanism for PF-LTD and its physiological occurrence is supported by *in vivo* receptive field plasticity [25]. This induction mechanism is novel, because our conditioning protocol substantially differs from that previously described [26], which consisted in a single EPSP repeated at 1 Hz for 5 minutes. In that study, the evidence that a single EPSP could already generate a calcium signal and the EPSCs reported (200 pA or larger) suggest that stronger stimulation intensities were used. This observation can account for two different mechanisms of LTP induction. In our conditions, we have shown that LTP induction is correlated with ECB saturation, which appears unnecessary in the tetanization protocol previously characterized [26].

Repetitive bursts of PF-EPSPs followed by 1 or 2 CF-EPSPs can induce PF-LTD [4,27] mediated by mGluR1 activation. The underlying pairing protocol occurs with a concomitant supra-linear calcium signal (Wang et al., 2000) associated with the CF-EPSP. However, as reported by Brenowitz and Regehr [12], not only is the dendritic component of this supra-linear calcium signal independent of mGluR1 activation and calcium release from stores, but the delay between PF and CF stimulation differs from that responsible for the mGluR1- and endocannabinoid-mediated short-term plasticity. Here we demonstrate that the CF-associated supra-linear $\Delta[Ca^{2+}]_i$ signal is also due to local ECB saturation.

Data reported in the **Supplementary Results** indicates that the priming calcium signal, necessary for $InsP_3$-mediated calcium release from stores [30] and generally provided by the CF-evoked spike [31], can be replaced by PF-evoked dendritic spikes. If this is the case, what is the mechanism of PF-CF coincident detection? We don't have an answer to this question, but the scenario appears to be a dynamic puzzle involving differences in calcium signaling [25] and other signaling aspects so far not investigated.

Calcium spikes decode the architecture of presynaptic fibers.

CGC axons ascend from their original layer and bifurcate perpendicularly to form beams of parallel trajectories extending for several millimeters. Synapses to PNs are formed both in the ascending tract [13] and through the parallel trajectories over long distances from the branching point [32]. Different biophysical mechanisms can interplay to decode the arrangement of presynaptic fibers into

postsynaptic signaling. A first mechanism is glutamate spillover that occurs only in adjacent synapses and regulates mGluR1 activation and LTD [17]. Here we show that the dendritic calcium burst is another mechanism that can decode the architecture of presynaptic fibers into synaptic plasticity. This property relies on the ability of PF/AF synapses to facilitate and elicit highly-localized calcium bursts, in contrast to the widespread CF-mediated dendritic spike.

In contrast to the mGluR1- and endocannabinoid-mediated LTD and to other forms of synaptic plasticity, that are exclusive of PF synapses [14,15,16], the LTP described here can also be induced by the sparser AF activation. Nevertheless, a difference in susceptibility for this type of plasticity cannot be excluded from the present experiments. In summary, glutamate spillover necessary for the activation of mGluR1 [17] and dendritic calcium bursts can decode the spatial organization of CGC-PN synapses at two different levels. The fine structure of PF-adjacent synapses can be decoded by the mGluR1 activation and by the local release of endocannabinoids leading to LTD. The gross structure of PF/AF synapses can be decoded by the local depolarization above the threshold for calcium firing leading to LTP.

METHODS

Slice preparation and electrophysiology

Experiments were done in 250 µm thick sagittal or in 300 µm thick coronal cerebellar slices from 25-35 days old mice (C57BL/6, body weight 10-19 g), decapitated following isoflurane anaesthesia (according to the Swiss regulation). Slices were prepared in ice-cold solution using a HM 650 V vibroslicer (Microm, Germany), incubated at 35 ^{0}C for 40 minutes and maintained at room temperature. Somatic whole-cell recordings were made at 32-34 ^{0}C using a Multiclamp 700A amplifier (Axon Instruments, USA) under an upright microscope (Olympus BX51-WI). For information on solution, recording protocols and analysis, see **Supplementary Methods**.

Statistical analysis

Results from two-sample or paired t-tests were considered significantly different for $p<0.01$ and not significantly different for $p>0.1$. In individual experiments, a conditioning protocol was defined to induce LTP or LTD when the p value of the two-sample t-test (N=20 samples) on the EPSP amplitudes before and after the conditioning protocol was <0.01.

Optical recordings

The procedure to achieve combined voltage and calcium recordings has been previously described [35,5]. Voltage and calcium fluorescence from 125 µm X 125µm (80X80 pixels) were sampled at 2000 frames/s and 500 frames/s respectively. Fractional changes of fluorescence were converted into ΔV_m as described in the **Supplementary Methods**. We estimated $\Delta[Ca^{2+}]_i$ from the

equation:

$$\Delta[Ca^{2+}]_i = K_d \cdot (F_0 - F)/F \quad (1)$$

where F is the fluorescence after auto-fluorescence subtraction and the fluorescence at 0 and saturating Ca^{2+} were approximated with the initial fluorescence (F_0) and with the auto-fluorescence respectively. We used K_d=10 µM for Fura-FF [34]. In this condition, the dye buffering capacity was negligible (only ~5%) compared to the estimated equilibrium ECB of the PN [20].

Two-photon imaging in coronal slices was done by scanning multiple sections to localize the dendritic site where the largest calcium signal was observed. Areas of typically 80-150 by 8 pixels were scanned at 17-25 Hz to measure local dendritic signals.

Detailed information on optical recordings is provided in the **Supplementary Methods**.

ACKNOWLEDGEMENTS

This work was supported by the University of Basel. We are grateful to Dejan Zecevic and Helene Pierre for technical help and to Anita Lüthi and Josef Kapfhammer for very valuable comments on the manuscript.

REFERENCES

1. Golding, N.L., Staff, N.P., & Spruston, N. Dendritic spikes as a mechanism for cooperative long-term potentiation *Nature* **418**, 326-331 (2002).

2. Holthoff K., Kovalchuk, Y., & Konnerth, A. Dendritic spikes and activity-dependent synaptic plasticity. *Cell Tissue Res.* **326**, 369-377 (2006).

3. Rancz, E.A., & Häusser, M. Dendritic calcium spikes are tunable triggers of cannabinoid release and short-term synaptic plasticity in cerebellar Purkinje neurons. *J. Neurosci.* **26**, 5428-5437 (2006).

4. Wang, S.S., Denk, W., & Häusser, M. Coincidence detection in single dendritic spines mediated by calcium release. *Nat. Neurosci.* **3**, 1266-1273 (2000).

5. Canepari M., Vogt, K., & Zecevic, D. Combining voltage and calcium imaging from neuronal dendrites. *Cell. Mol. Neurobiol.* DOI 10.1007/s10571-008-9287-9 (2008).

6. Kuruma, A., Inoue, T., & Mikoshiba, K. Dynamics of Ca^{2+} and Na^{+} in the dendrites of mouse cerebellar Purkinje cells evoked by parallel fibre stimulation. *Eur. J. Neurosci.* **18**, 2677-2689 (2003).

7. Stuart, G., & Hausser, M. Initiation and spread of sodium action potentials in cerebellar Purkinje cells. *Neuron* **13**, 703-712 (1994).

8. Renzi, M., Farrant, M., & Cull-Candy, S.G. Climbing-fibre activation of NMDA receptors in Purkinje cells of adult mice. *J. Physiol.* **585**, 91-101 (2007).

9. Miyakawa, H., Lev-Ram, V., Lasser-Ross, N., & Ross, W.N. Calcium transients evoked by climbing fiber and parallel fiber synaptic inputs in guinea pig cerebellar Purkinje neurons. *J. Neurophysiol.* **68**, 1178-1189 (1992).

10. Dittman, J.S., & Regehr, W.G. Calcium dependence and recovery kinetics of presynaptic depression at the climbing fiber to Purkinje cell synapse. *J. Neurosci.* **18**, 6147-6162 (1998).

11. Silver, R.A., Momiyama, A., & Cull-Candy, S.G. Locus of frequency-dependent depression identified with multiple-probability fluctuation analysis at rat climbing fibre-Purkinje cell synapses. *J. Physiol.* **510**, 881-902 (1998).

12. Brenowitz, S.D., & Regehr, W.G. Associative short-term synaptic plasticity mediated by endocannabinoids. *Neuron* **45**, 419-431 (2005).

13. Gundappa-Sulur, G., De Schutter, E., & Bower, J.M. Ascending granule cell axon: an important component of cerebellar cortical circuitry. *J. Comp. Neurol.* **408**, 580-596 (1999).

14. Sims R.E., & Hartell N.A. Differences in transmission properties and susceptibility to long-term depression reveal functional specialization of ascending axon and parallel fiber synapses to Purkinje cells. *J. Neurosci.* **25**, 3246-3257 (2005).

15. Sims R.E., & Hartell N.A. Differential susceptibility to synaptic plasticity reveals a functional specialization of ascending axon and parallel fiber synapses to cerebellar Purkinje cells. *J. Neurosci.* **26**, 5153-5159 (2006).

16. Marcaggi, P., & Attwell, D. Short- and long-term depression of rat cerebellar parallel fibre synaptic transmission mediated by synaptic crosstalk. *J. Physiol.* **578**, 545-550. (2007).

17. Marcaggi, P., & Attwell, D. Endocannabinoid signaling depends on the spatial pattern of synapse activation. *Nat. Neurosci.* **8**, 776-781 (2005).

18. Neher, E. Usefulness and limitations of linear approximations to the understanding of Ca++ signals. *Cell Calcium* **24**, 345-357 (1998).

19. Blatow, M., Rozov, A., Katona, I., Hormuzdi, S.G, Meyer, A.H., Whittington, M.A., Caputi, A., & Monyer, H. Ca2+ buffer saturation underlies paired pulse facilitation in calbindin-D28k-containing terminals. *Neuron* **38**, 79-88 (2003).

20. Fierro, L., & Llano, I. High endogenous calcium buffering in Purkinje cells from rat cerebellar slices. *J. Physiol.* **496**, 617-625 (1996).

21. Lee, S.H., Schwaller, B., & Neher, E. Kinetics of Ca2+ binding to parvalbumin in bovine chromaffin cells: implications for [Ca2+] transients of neuronal dendrites. *J. Physiol.* **525**, 419-432 (2000).

22. Nägerl U.V., Novo, D., Mody, I., & Vergara, J.L. Binding kinetics of calbindin-D(28k) determined by flash photolysis of caged Ca(2+). *Biophys. J.* **79**, 3009-3018 (2000).

23. Celio, M.R. (1990). Calbindin D-28k and parvalbumin in the rat nervous system. Neuroscience *35*, 375-475.

24. Müller, M., Felmy, F., Schwaller, B., & Schneggenburger, R. Parvalbumin is a mobile presynaptic Ca2+ buffer in the calyx of held that accelerates the decay of Ca2+ and short-term facilitation. *J. Neurosci.* **27**, 2261-2271 (2007).

25. Jörntell, H., & Hansel, C. Synaptic memories upside down: bidirectional plasticity at cerebellar parallel fiber-Purkinje cell synapses. *Neuron* **52**, 227-238 (2006).

26. Coesmans, M., Weber, J.T., De Zeeuw, C.I., & Hansel, C. Bidirectional parallel fiber plasticity in the cerebellum under climbing fiber control. *Neuron* **18**, 691-700 (2004).

27. Safo, P.K., & Regehr, W.G. Endocannabinoids control the induction of cerebellar LTD. *Neuron* **48**, 647-659 (2006).

28. Finch, E.A., & Augustine, G.J. Local calcium signalling by inositol-1,4,5-trisphosphate in Purkinje cell dendrites. *Nature* **396**, 753-756 (1998).

29. Takechi, H., Eilers, J., & Konnerth, A. A new class of synaptic response involving calcium release in dendritic spines. *Nature* **396**, 757-760 (1998).

30. Canepari M., & Ogden, D. Kinetic, pharmacological and activity-dependent separation of two Ca2+ signalling pathways mediated by type 1 metabotropic glutamate receptors in rat Purkinje neurones. *J. Physiol.* **573**, 65-82 (2006).

31. Sarkisov, D.V., & Wang, S.S. Order-dependent coincidence detection in cerebellar Purkinje neurons at the inositol trisphosphate receptor. *J. Neurosci.* **28**, 133-142 (2008).

32. Coutinho, V., Mutoh, H., & Knöpfel, T. Functional topology of the mossy fibre-granule cell--Purkinje cell system revealed by imaging of intrinsic fluorescence in mouse cerebellum. *Eur. J. Neurosci.* **20**, 740-748 (2004).

33. Canepari M., Djurisic, M., & Zecevic, D. Dendritic signals from rat hippocampal CA1 pyramidal neurons during coincident pre- and post-synaptic activity: a combined voltage- and calcium-imaging study. *J. Physiol.* **580**, 463-484 (2007).

34. Schneggenburger, R., & Neher, E. Intracellular calcium dependence of transmitter release rates at a fast central synapse. *Nature* **406**, 889-893 (2000).

FIGURE LEGENDS

Figure *1* Dendritic ΔV_m and $\Delta[Ca^{2+}]_i$ associated with PF-EPSPs **(a)** PN reconstruction (left) and recorded dendrites with three sample regions (8X8 pixels) and the position of the stimulating electrode; peak ΔV_m and $\Delta[Ca^{2+}]_i$ signals following 10 PF-EPSPs at 100 Hz represented with color-coded scales. **(b)** ΔV_m and $\Delta[Ca^{2+}]_i$ signals associated with 3, 5, 7 and 10 PF-EPSPs in the three regions; somatic recordings reported; peak ΔV_m > 40 mV and detectable $\Delta[Ca^{2+}]_i$ signals only in region 1. **(c)** Peak ΔV_m corresponding to 1-10 EPSPs and peak $\Delta[Ca^{2+}]_i$ following 3, 5, 7 and 10 EPSPs from 5 PNs; each symbol represents a different cell. **(d)** PN reconstruction (right) and recorded dendrites with the 8X8 pixel region of maximal $\Delta[Ca^{2+}]_i$ signal; peak ΔV_m and $\Delta[Ca^{2+}]_i$ signals following 7 PF-EPSPs at 100 Hz represented in color-code. **(e)** (Left) - ΔV_m and $\Delta[Ca^{2+}]_i$ recordings from the region in d following 7 PF-EPSPs; $\Delta[Ca^{2+}]_i$ recording following 3 PF-EPSPs reported above; normalized $\Delta[Ca^{2+}]_i$ recordings with 3 and 7 PF-EPSPs reported below. (Right) - Peak ΔV_m and $\Delta[Ca^{2+}]_i$ signals corresponding to the 3rd and 7th EPSP; normalized peak $\Delta[Ca^{2+}]_i$ signals corresponding to the 3rd and 7th EPSP superimposed and single exponential decay fit (20 ms) reported below. **(f)** Fractional changes (Mean ± SD, N = 8 cells) of the 7th peak ΔV_m relative to the 3rd peak, of the peak 7-EPSPs $\Delta[Ca^{2+}]_i$ relative to the peak 3-EPSPs $\Delta[Ca^{2+}]_i$ and of the 7-EPSPs $\Delta[Ca^{2+}]_i$ decay time constant (τ_7) relative to the 3-EPSPs $\Delta[Ca^{2+}]_i$; decay time constant (τ_3).

Figure *2* Dendritic ΔV_m and $\Delta[Ca^{2+}]_i$ increasing the number of stimulated PFs. **(a)** PN reconstruction (right) and recorded dendrites (left) with three sample regions (1-3) and the whole dendritic regions indicated. Peak ΔV_m and $\Delta[Ca^{2+}]_i$ following 7 PF-EPSPs at 100 delivered by the electrode "stim" at a "weak" and "strong" stimulation intensities represented in color-code. **(b)** ΔV_m and $\Delta[Ca^{2+}]_i$ recordings from the regions 1-3 following PF stimulation at the two stimulation intensities; somatic recordings also reported. **(c)** ΔV_m corresponding to the last two spikes following weak and strong PF stimulation. **(d)** Scatter plot of peak $\Delta[Ca^{2+}]_i$ against peak ΔV_m averaged over the last three spikes at two stimulation intensities from 7 cells; empty symbols: weak stimulation; filled symbols: strong stimulation; each symbol represents a different cell.

Figure *3* Dendritic ΔV_m and $\Delta[Ca^{2+}]_i$ associated with CF-EPSPs. **(a)** (Left) – PN reconstruction and recorded dendrites with three sample regions (1-3) and the whole dendritic regions (*whole*) indicated. (Right) - ΔV_m and $\Delta[Ca^{2+}]_i$ associated with 1 CF-EPSP or 5 CF-EPSPs at 100 Hz in the regions 1,2,3 and *whole*; somatic recordings reported. **(b)** Mean ± SD of the peak ΔV_m associated with 5 CF-EPSPs at 100 Hz and of the peak $\Delta[Ca^{2+}]_i$ associated with 1 CF-EPSP and 5 CF-EPSPs at 100 Hz from 4 PNs over the imaged dendritic area. **(c)** (Left) - PN reconstruction and recorded dendrites with three sample regions (1-3); peak ΔV_m and $\Delta[Ca^{2+}]_i$ following 7 PF-EPSPs at 100 Hz delivered by "stim" represented in color-code. (Right) - Corresponding $\Delta[Ca^{2+}]_i$ recordings from the regions 1-3; somatic recording reported. **(d)** ΔV_m and $\Delta[Ca^{2+}]_i$ in the regions 1-3 following 1

CF EPSP unpaired (CF) and paired to 7 PF-EPSPs with a delay of 90 ms; paired CF-mediated $\Delta[Ca^{2+}]_i$ signal larger in the region excited by the PF-EPSPs. **(e)** (Left) – ΔV_m associated with the CF-EPSP in unpaired and paired conditions; no change in the CF ΔV_m signal. (Right) – Supra-linear $\Delta[Ca^{2+}]_i$ from the difference between $\Delta[Ca^{2+}]_i$ associated with the pairing protocol and $\Delta[Ca^{2+}]_i$ associated with the unpaired PF-EPSPs and CF-EPSP; color-coded image is the supra-linear $\Delta[Ca^{2+}]_i$. **(f)** Mean ± SD of the peak CF ΔV_m and $\Delta[Ca^{2+}]_i$ associated 1 CF-EPSP unpaired or paired to 7 PF-EPSPs from 6 PNs; two populations t-tests: ΔV_m signals, $p>0.1$; $\Delta[Ca^{2+}]_i$ signals, $p<0.01$.

Figure *4* Repetitive PF-EPSPs bursts induce PF-LTP. **(a)** PN reconstruction. **(b)** (Top) – Recorded dendrites with the position of two stimulating electrodes (s1 and s2) and the mean $\Delta[Ca^{2+}]_i$ peak associated with repetitive 3-EPSPs bursts (3p) and 7-EPSPs bursts (7p) delivered by s1 represented in color-code. (Bottom) - $\Delta[Ca^{2+}]_i$ recordings in the maximal 8X8 pixels region and somatic recordings associated with 3p (left) and 7p (right) protocols. **(c)** Average of 20 recordings following s1 and s2 stimulation in control, 10-15 minutes after the 3p protocol and 10-15 minutes after 7p protocol. **(d)** Time course of EPSP amplitudes normalized to control EPSP amplitudes (20 EPSPs in 5 minutes) evoked by s1 and s2; each point is the average of 4 EPSPs in one minute; the arrows indicate the time of the 3p and 7p protocols. **(e)** (Top) - Scatter plot of mean normalized EPSP 10-15 after a 3p protocol and after a 7p protocol against peak $\Delta[Ca^{2+}]_i$; each symbol is a different cell. (Bottom) - Mean ± SD of

normalized EPSP 10-15 minutes after a 3p protocol and 10-15 after a 7p protocol; paired t-test: $p<0.01$.

Figure *5* PF-evoked PF long term plasticity depends on the $\Delta[Ca^{2+}]_i$ peak. **(a)** (Left) – PN reconstruction and recorded dendrites tree with the position of stimulating electrodes s1 and s2 and the $\Delta[Ca^{2+}]_i$ peak following a conditioning protocol delivered by s1 in color-code. (Right) - $\Delta[Ca^{2+}]_i$ signal of ~250 nM in its maximal 8X8 pixels region (average of 30 trials). **(b)** Time course of the normalized EPSP amplitudes (20 EPSPs in 5 minutes) evoked by s1 and s2; each point is the average of 4 EPSPs; the arrow indicates the s1 conditioning protocol; traces are averages of 20 EPSPs before, 5-10 minutes after and 15-20 minutes after the conditioning protocol. **(c and d)** Same as a and b in another cell with mean $\Delta[Ca^{2+}]_i$ ~1 µM. **(e and f)** Same as a and b in another cell with mean $\Delta[Ca^{2+}]_i$ ~2 µM. **(g)** (Bottom) - Semi-logarithmic scatter plot of mean normalized EPSP 5-10 after the conditioning protocol against peak $\Delta[Ca^{2+}]_i$ during the conditioning protocol; values in control condition: 35 cells and 45 dendritic locations; CPCCOEt (100 µM): 12 dendritic locations; LY367385 (100 µM): 12 dendritic locations; AP5 (100 µM): 13 dendritic locations; bicuculline (20 µM): 10 dendritic locations. (Top) - Mean ± SD of normalized EPSP 5-10 minutes after conditioning protocol in the ranges of 0.1-0.4 µM $\Delta[Ca^{2+}]_i$, of 0.4-1.5 µM $\Delta[Ca^{2+}]_i$ and of 2-4 µM $\Delta[Ca^{2+}]_i$. **(h)** Mean ± SD of normalized EPSP 15-20 minutes after conditioning protocol in the range of 0.4-1.5 µM $\Delta[Ca^{2+}]_i$.

Figure *6* Postsynaptic induction of PF-LTP. **(a)** (Top) - Alexa-488 fluorescence from a PN 10 minutes (left) and 45 minutes (right) after whole cell; the pipette filled from the tip with clear solution and from the back with 25 mM BAPTA and 100 µM Alexa-488. (Bottom) – Corresponding Fura-FF fluorescence from the same PN; $\Delta[Ca^{2+}]_i$ peak following 7 stimuli delivered by s1 and s2 represented in color code. **(b)** Time course of normalized EPSP amplitudes evoked by s1 and s2 (20 EPSPs in 5 minutes); the arrows indicate the time of the conditioning protocols. **(c)** (Left) - Scatter plot of the mean normalized EPSP 5-10 after conditioning protocol against the peak $\Delta[Ca^{2+}]_i$ associated with a conditioning protocol; control condition, 13 dendritic locations tested; 25 mM BAPTA (5 cells and 6 dendritic locations tested). (Right) - Mean ± SD of normalized EPSP 5-10 minutes after a conditioning protocol in the range of 0.4-1 µM $\Delta[Ca^{2+}]_i$; two-sample t-test (control and BAPTA experiments): $p<0.01$.

Figure *7* Dendritic PF and AF $\Delta[Ca^{2+}]_i$ signals in coronal slices. **(a)** (Left) - Schematic of a sagittal/coronal section of the cerebellum with Molecular Layer (ML), PN Layer (PNL) and Granule Cell layer (GCL); PF stimulation: stimulation in the ML ~150 µm from the dendritic plane; AF stimulation: stimulation in the GCL behind the PN. (Right) - 3D reconstruction of a PN in a coronal slice; the angle α from the plane of the slice indicated. **(b)** Relative calibration of fractional fluorescence changes of Fura-FF and OG-5N. (Top) - Recordings from 1 cell, 2 stimulation intensities. (Bottom) - Scatter plot from 4 cells, 2 stimulation intensities, each symbol represents a cell; linear least square fit indicated. **(c)**

Region in the coronal section of a PN dendritic tree (top) and color-coded peak $\Delta[Ca^{2+}]_i$ (bottom) superimposed over the fluorescence image associated with PF stimulation at three stimulation intensities. (**d**) - $\Delta[Ca^{2+}]_i$ recordings from the region in the top image and corresponding somatic recordings at different time scales. **(e)** - Scatter plot of peak $\Delta[Ca^{2+}]_i$ following PF stimulation against the amplitude of the first EPSP; each symbol is a different cell; $\Delta[Ca^{2+}]_i$ signals corresponding to a first EPSP of 3-6 mV in the range of LTP induction. **(f, g and h)** Same as (c, d and e) in cells where EPSPs and $\Delta[Ca^{2+}]_i$ signals were elicited by AF stimulation; $\Delta[Ca^{2+}]_i$ signals in the range of LTP induction.

Figure *8* PF-LTP and AF-LTP in coronal slices. **(a)** (Top) - Averaged EPSP traces following PF stimulation in coronal slices before, 5 to 10 minutes after and 15-20 minutes after a conditioning protocol. (Bottom) - Time course over 6 cells (Mean ± SD) of the normalized EPSP in the range of 3-6 mV before and after a condition protocol; white symbols: control internal solution; colored symbols: 25 mM BAPTA. **(b)** Mean ± SD over 20 EPSPs evoked 5-10 minutes and 15-20 minutes after a conditioning protocol; experiments with control solution (N=6 cells) and with 25 mM BAPTA in the pipette (N=6 cells); two-sample t-test (control and BAPTA experiments): $p<0.001$. **(c and d)** Same as (a and b) in cells where EPSPs were elicited by AF stimulation; experiments with control internal solution (N=6 cells) and with 25 mM BAPTA (N=6 cells); two-sample t-test (control and BAPTA experiments): $p<0.001$.

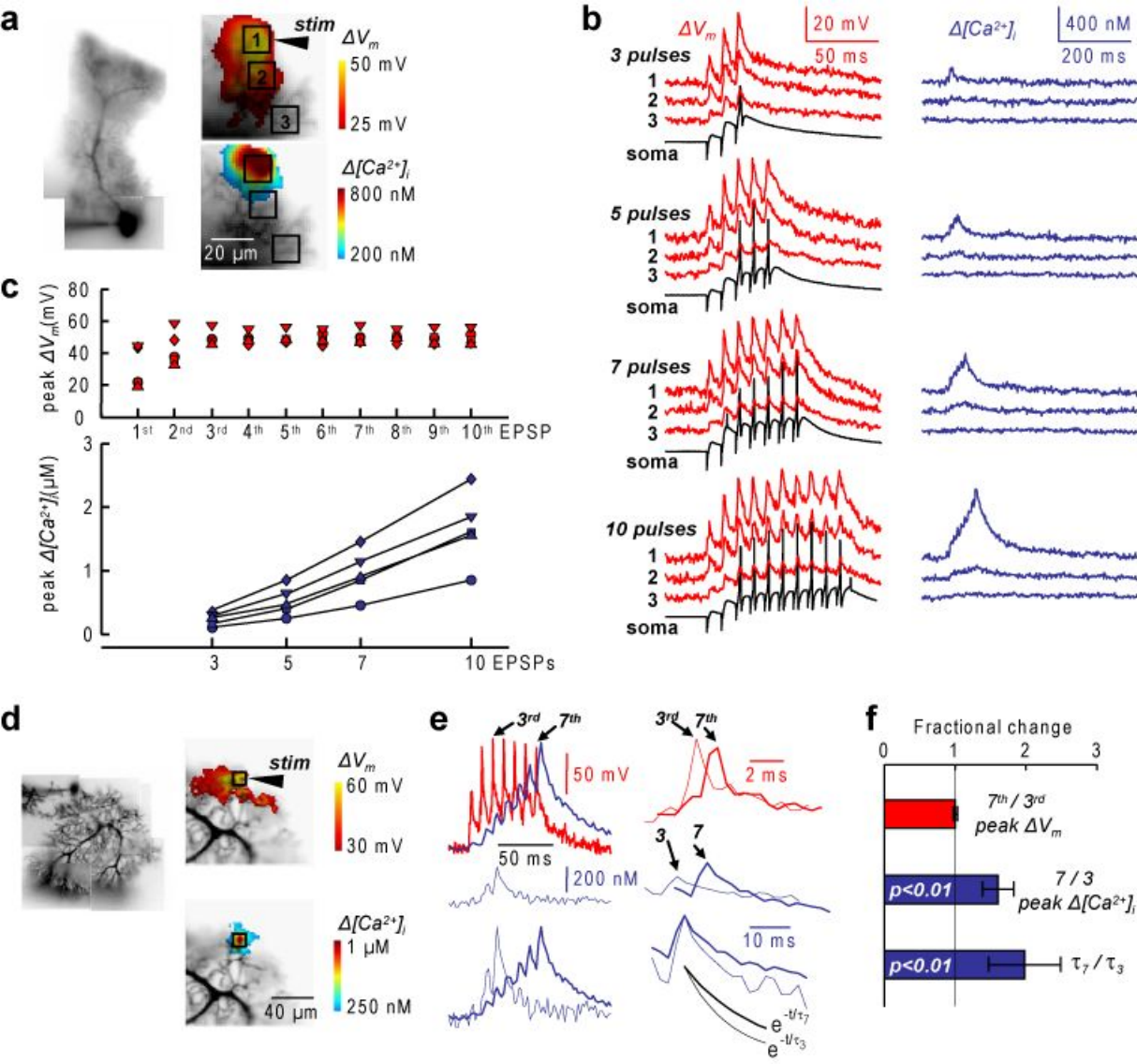
a
stim
1
2
3
ΔVm
50 mV
25 mV
Δ[Ca2+]i
800 nM
200 nM
20 μm
b
ΔVm
20 mV
50 ms
Δ[Ca2+]i
400 nM
200 ms
3 pulses
5 pulses
7 pulses
10 pulses
soma
c
peak ΔVm (mV)
1st 2nd 3rd 4th 5th 6th 7th 8th 9th 10th EPSP
peak Δ[Ca2+]i (μM)
3 5 7 10 EPSPs
d
stim
ΔVm
60 mV
30 mV
Δ[Ca2+]i
1 μM
250 nM
40 μm
e
3rd 7th
50 mV
50 ms
200 nM
2 ms
3
7
10 ms
f
Fractional change
0 1 2 3
7th / 3rd peak ΔVm
p<0.01
7 / 3 peak Δ[Ca2+]i
p<0.01
τ7 / τ3

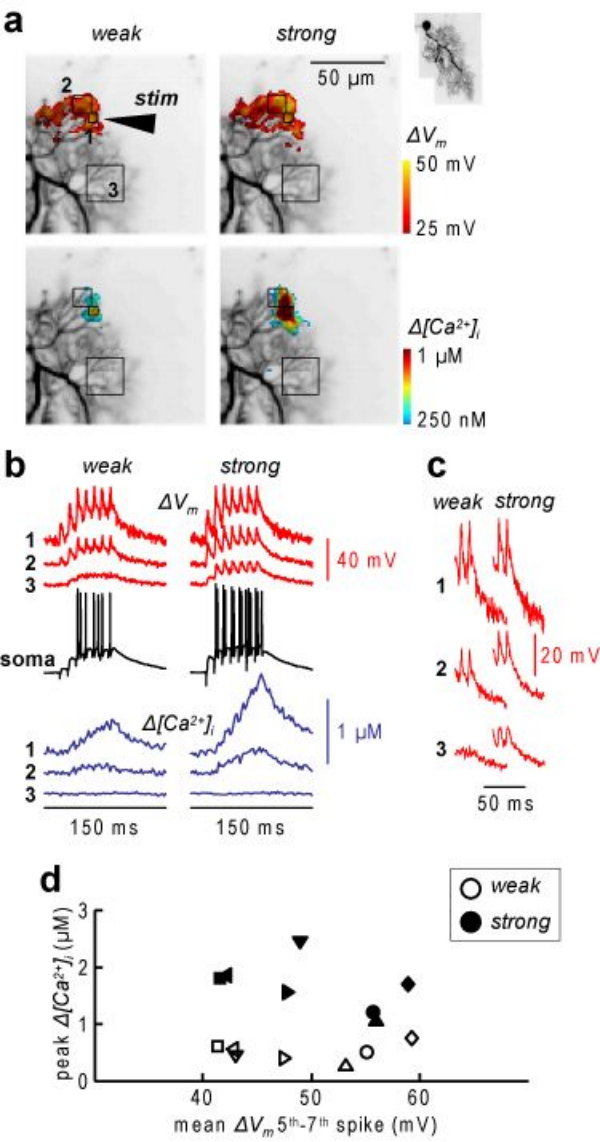
a
weak
strong
50 µm
2
stim
3
ΔVm
50 mV
25 mV
Δ[Ca2+]i
1 µM
250 nM
b
weak
strong
ΔVm
1
2
3
40 mV
soma
Δ[Ca2+]i
1 µM
150 ms
150 ms
c
weak
strong
1
2
3
20 mV
50 ms
d
weak
strong
peak Δ[Ca2+]i (µM)
mean ΔVm 5th-7th spike (mV)

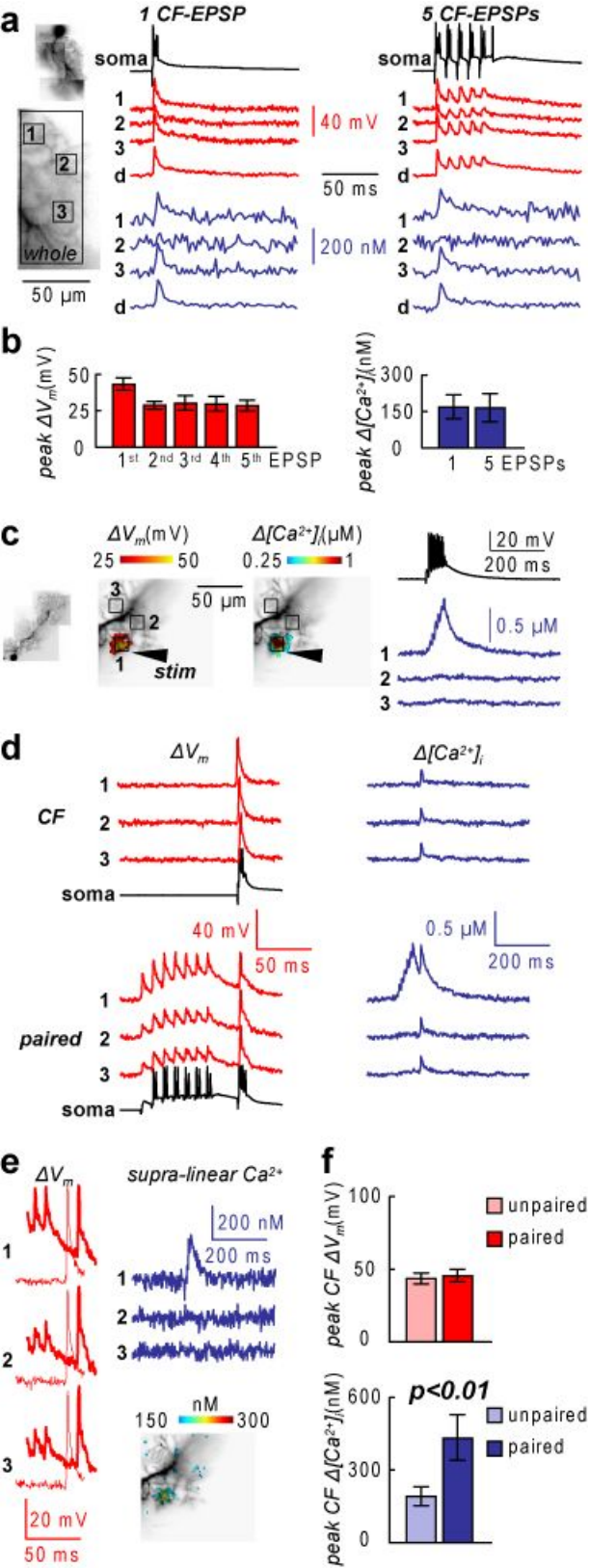
a
1 CF-EPSP
5 CF-EPSPs
soma
1
2
3
d
40 mV
50 ms
200 nM
whole
50 µm
b
peak ΔVm(mV)
50
25
0
1st 2nd 3rd 4th 5th EPSP
peak Δ[Ca2+]i(nM)
300
150
0
1
5 EPSPs
c
ΔVm(mV)
25
50
Δ[Ca2+]i(µM)
0.25
1
50 µm
stim
20 mV
200 ms
0.5 µM
d
ΔVm
Δ[Ca2+]i
CF
paired
soma
40 mV
50 ms
0.5 µM
200 ms
e
ΔVm
supra-linear Ca2+
200 nM
200 ms
nM
150
300
20 mV
50 ms
f
peak CF ΔVm(mV)
100
50
0
unpaired
paired
p<0.01
peak CF Δ[Ca2+]i(nM)
600
300
0
unpaired
paired

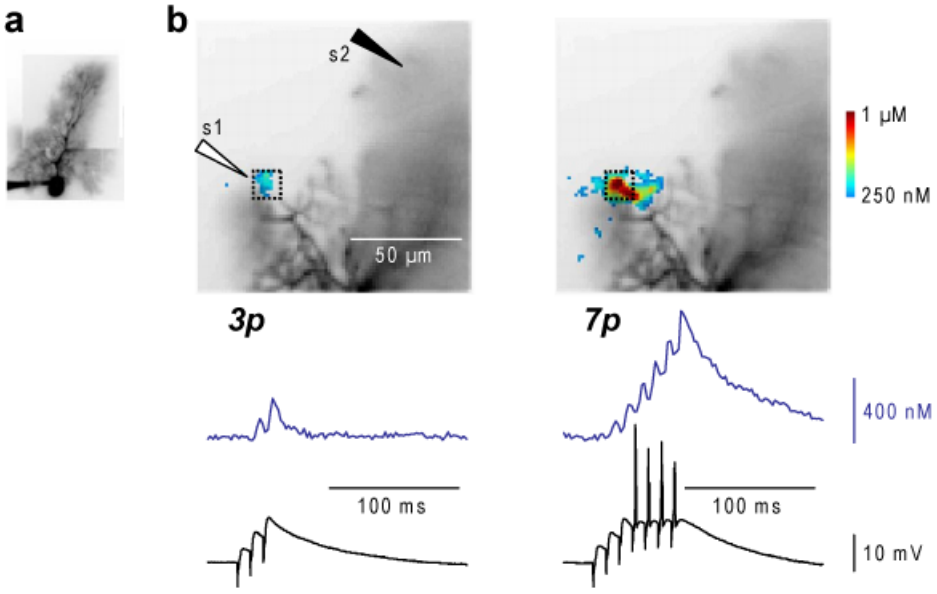
a
b
s2
s1
50 µm
1 µM
250 nM
3p
7p
400 nM
100 ms
100 ms
10 mV

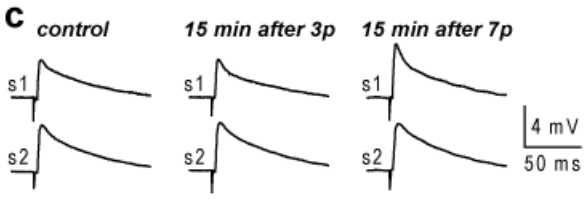
c
control
15 min after 3p
15 min after 7p
s1
s2
4 mV
50 ms

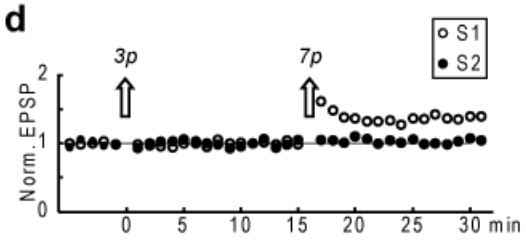
d
3p
7p
S1
S2
Norm. EPSP
0
5
10
15
20
25
30 min

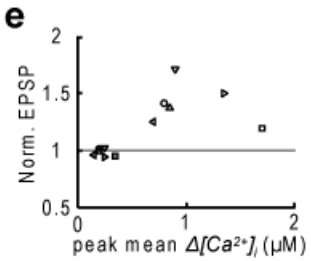
e
Norm. EPSP
peak mean Δ[Ca2+]i (µM)
10-15 min after 3p
10-15 min after 7p
p<0.01
Norm. EPSP (15-20 min)

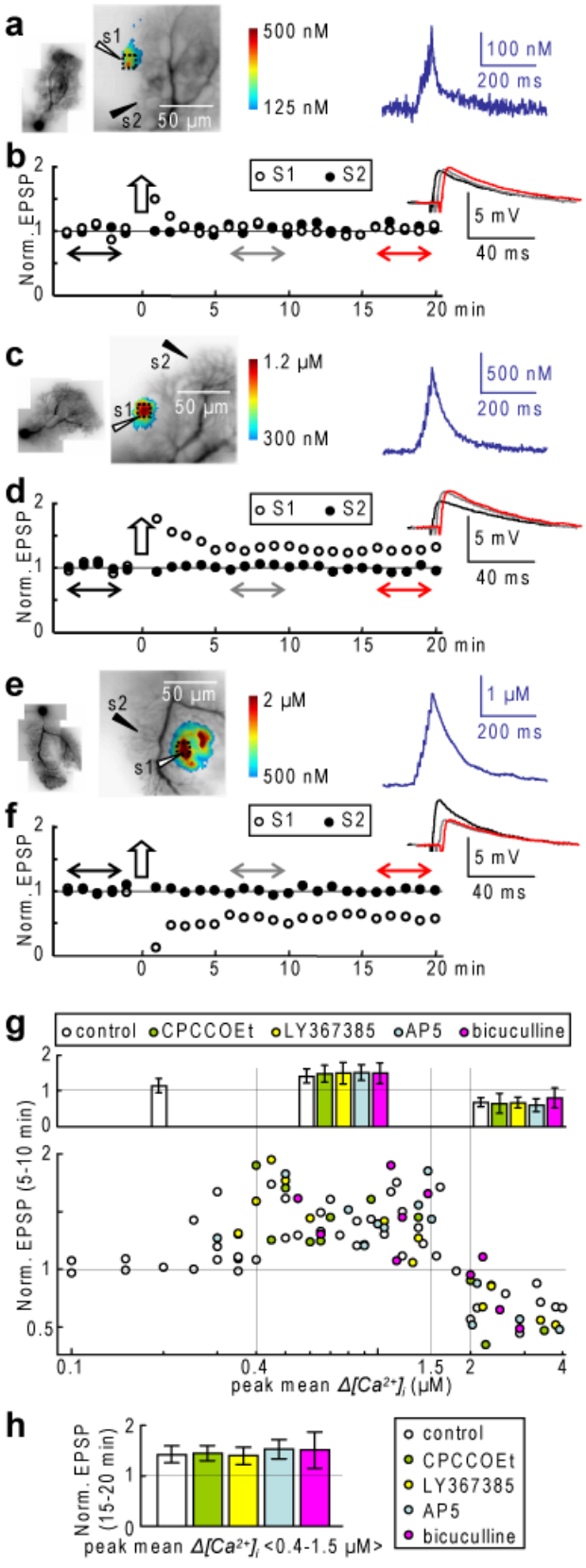
a
s1
s2
50 µm
500 nM
125 nM
100 nM
200 ms
b
S1
S2
Norm. EPSP
5 mV
40 ms
0
5
10
15
20 min
c
s2
s1
50 µm
1.2 µM
300 nM
500 nM
200 ms
d
S1
S2
Norm. EPSP
5 mV
40 ms
0
5
10
15
20 min
e
50 µm
s2
s1
2 µM
500 nM
1 µM
200 ms
f
S1
S2
Norm. EPSP
5 mV
40 ms
0
5
10
15
20 min
g
control
CPCCOEt
LY367385
AP5
bicuculline
Norm. EPSP (5-10 min)
0.1
0.4
1.5
2
4
peak mean Δ[Ca2+]i (µM)
h
Norm. EPSP (15-20 min)
peak mean Δ[Ca2+]i <0.4-1.5 µM>
control
CPCCOEt
LY367385
AP5
bicuculline

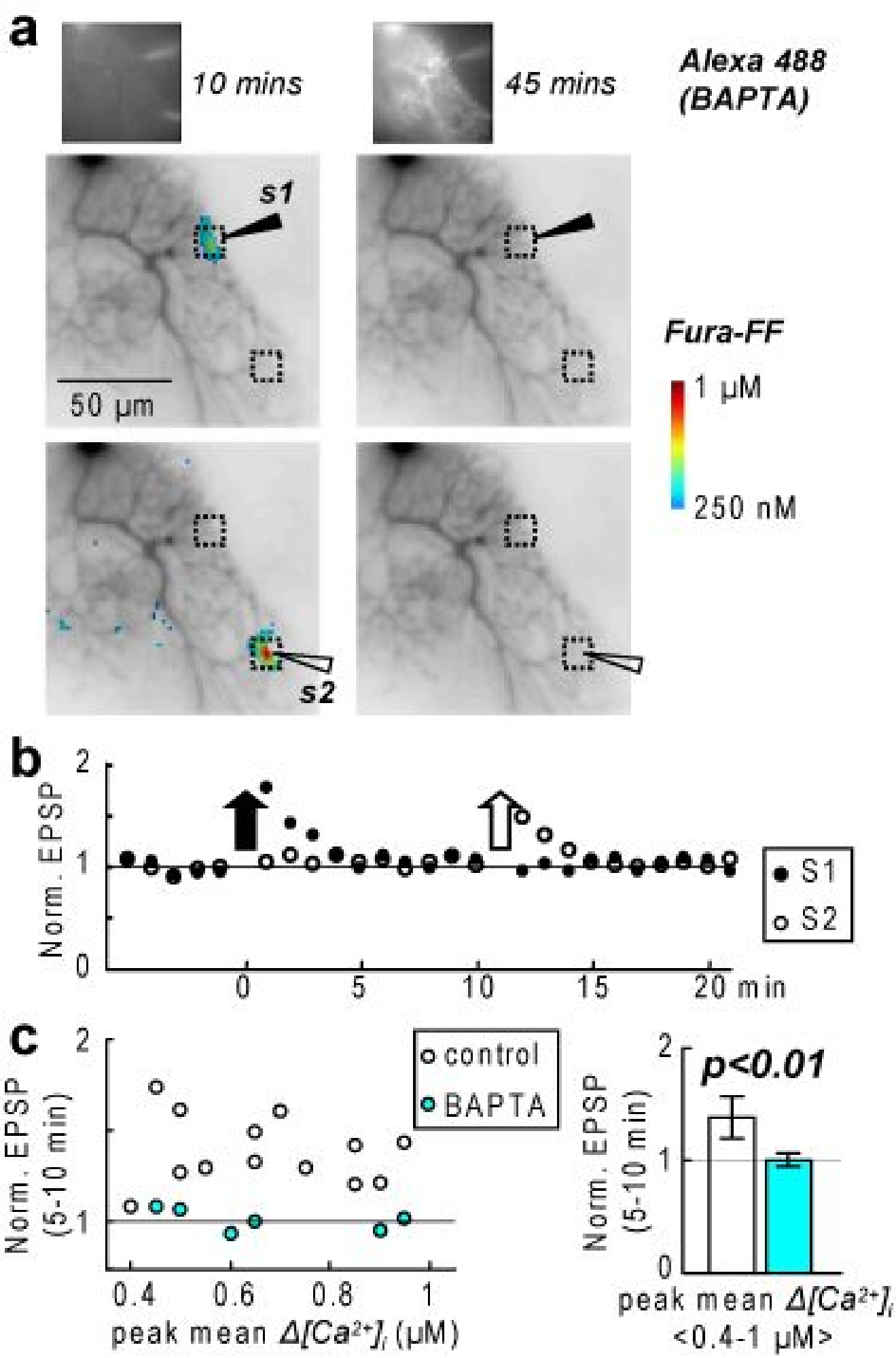
a
10 mins
45 mins
Alexa 488
(BAPTA)
s1
50 µm
Fura-FF
1 µM
250 nM
s2
b
Norm. EPSP
2
1
0
0
5
10
15
20 min
S1
S2
c
Norm. EPSP
(5-10 min)
2
1
control
BAPTA
0.4
0.6
0.8
1
peak mean Δ[Ca2+]i (µM)
p<0.01
Norm. EPSP
(5-10 min)
2
1
0
peak mean Δ[Ca2+]i
<0.4-1 µM>

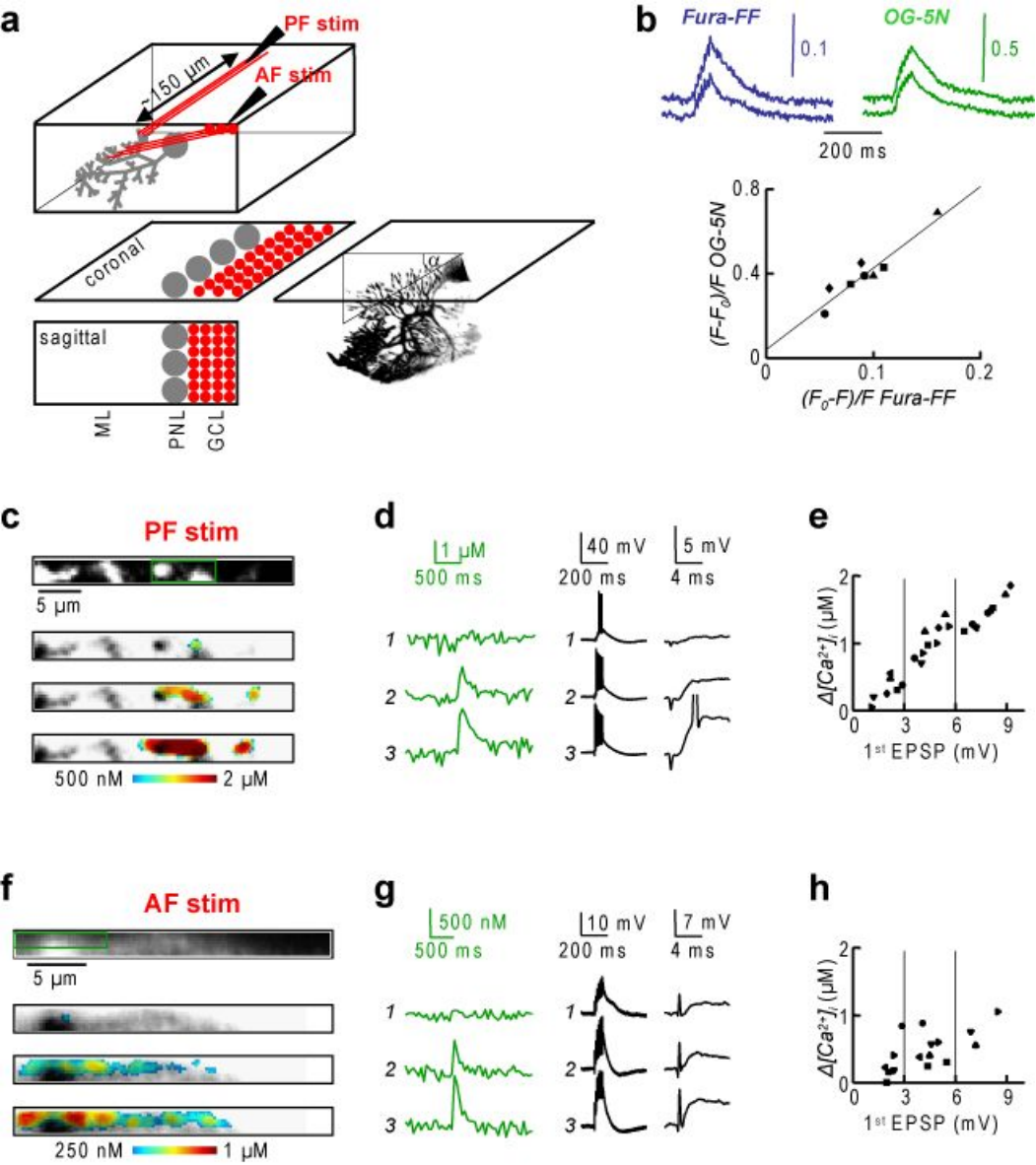
a
PF stim
~150 µm
AF stim
coronal
sagittal
ML
PNL
GCL
α
b
Fura-FF
OG-5N
0.1
0.5
200 ms
0.8
0.4
0
0.1
0.2
(F-F0)/F OG-5N
(F0-F)/F Fura-FF
c
PF stim
5 µm
500 nM
2 µM
d
1 µM
500 ms
40 mV
200 ms
5 mV
4 ms
1
2
3
e
Δ[Ca2+]i (µM)
2
1
0
0
3
6
9
1st EPSP (mV)
f
AF stim
5 µm
250 nM
1 µM
g
500 nM
500 ms
10 mV
200 ms
7 mV
4 ms
1
2
3
h
Δ[Ca2+]i (µM)
2
1
0
0
3
6
9
1st EPSP (mV)

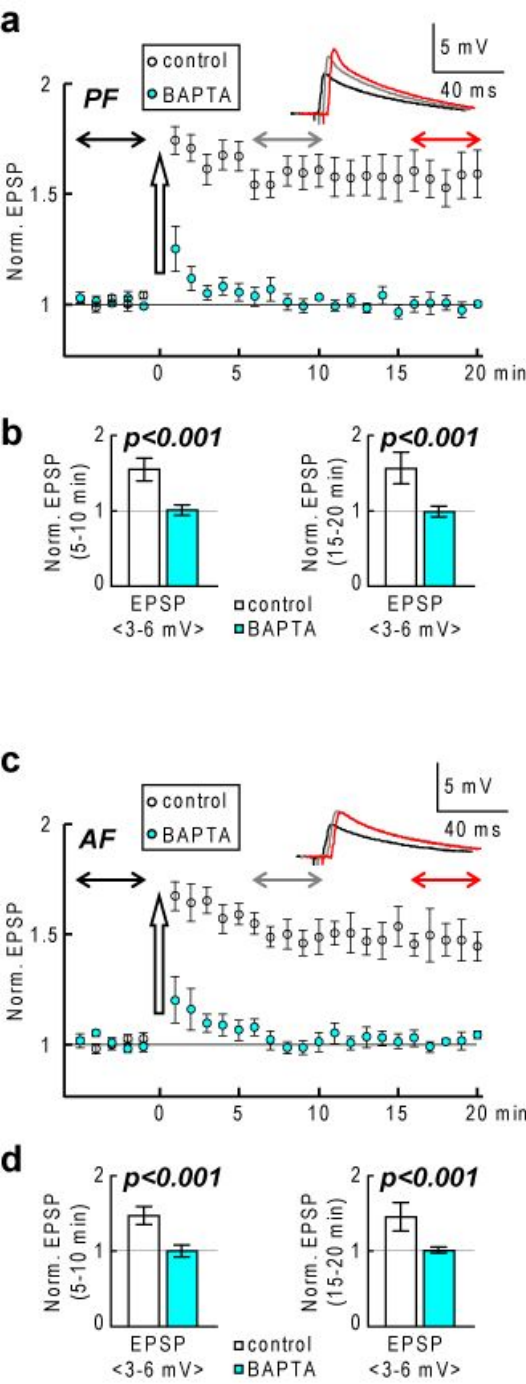
a
control
BAPTA
PF
5 mV
40 ms
Norm. EPSP
2
1.5
1
0
5
10
15
20 min
b
p<0.001
Norm. EPSP (5-10 min)
Norm. EPSP (15-20 min)
EPSP <3-6 mV>
control
BAPTA
c
AF
d